

## 높은 투명도와 강도를 갖는 자가치료용 Polyurethane: 복합 초분자 상호작용의 영향

Yuan Liu, Yanmei Liao\*, Yintao Long\*, Yuxiang Qian\*\*, Shengqiang Nie, Yi Wang,  
Jia Zeng, Chunmei Zhang, Linbo Tian, and Jun Luo<sup>†</sup>

Engineering Research Center for Materials Protection of Wear and Corrosion of Guizhou Province, Guiyang University

\*State Key Laboratory Breeding Base of Green Pesticide and Agricultural Bioengineering, Key Laboratory of Green Pesticide and Agricultural Bioengineering, Ministry of Education, Center for R&D of Fine Chemicals, Guizhou University

\*\*Shanghai Space Propulsion Technology Research Institute

(2021년 11월 16일 접수, 2022년 3월 1일 수정, 2022년 3월 12일 채택)

## A Novel Self-Healing Polyurethane with High Transparency and Strength: Effects of Multiple Supermolecular Forces

Yuan Liu, Yanmei Liao\*, Yintao Long\*, Yuxiang Qian\*\*, Shengqiang Nie, Yi Wang,  
Jia Zeng, Chunmei Zhang, Linbo Tian, and Jun Luo<sup>†</sup>

Engineering Research Center for Materials Protection of Wear and Corrosion of Guizhou Province,  
Guiyang University, Guiyang 550005, China

\*State Key Laboratory Breeding Base of Green Pesticide and Agricultural Bioengineering, Key Laboratory of Green Pesticide and Agricultural Bioengineering, Ministry of Education, Center for R&D of Fine Chemicals, Guizhou University,  
Guiyang 550025, China

\*\*Shanghai Space Propulsion Technology Research Institute, No. 3888, Yuanjiang Road, Minhang District, Shanghai 201100, China

(Received November 16, 2021; Revised March 1, 2022; Accepted March 12, 2022)

**Abstract:** It is a considerable challenge for expanding the applications of self-healing polyurethane because of the dilemma in balancing its mechanical and self-healing properties. Herein, a series of self-healing polyurethane systems (PUT-*x*) with short-range ordered rigid aromatic structures were synthesized by simply adjusting two kinds of diisocyanates, and by ingenious addition of aromatic chain extender. We hope to regulate the  $\pi$ - $\pi$  interactions and further to manipulate the properties of obtained polyurethanes via adjusting the amount of the benzene rings in the molecular chains of the PUT-*x* systems. The PUT-5 with decent self-healing ability, optimal mechanical properties, acceptable thermal stability and favorable transparency was selected to incorporate liquid metal and fluorescent powder to fabricate conductive wire and anti-counterfeiting film. Significantly, the liquid metal could be recycled from the conductive wire conveniently without using strong acids or strong bases. Moreover, PUT-5 exemplarily withstood long-term soaking in normal saline, and no deformation could be identified.

**Keywords:** self-healing, polyurethane,  $\pi$ - $\pi$  interaction, hydrogen bond, properties.

### Introduction

With the development of human society, impressive progresses have been achieved in design, synthesis, and application of the polymer materials. Meanwhile, such progresses also have benefited human beings considerably in recent decades.<sup>1</sup> However, the polymer materials, compared with

metal materials, are easier to suffer from mechanical damage, which results in loss of their proper functions.<sup>2</sup> Therefore, countless efforts have been devoted to preparing self-healing polymers, including thermoplastics and thermosets such as polydimethylsiloxane,<sup>3,4</sup> epoxy,<sup>5,6</sup> polyurethane,<sup>7,8</sup> and so on. To establish desired self-healing polymers, the prerequisite is to introduce appropriate dynamic covalent and/or noncovalent bonds into the chemical structures of the polymers. Dynamic covalent bonds that usually are applied to prepare self-healing polymers include boronic ester linkage,<sup>9,10</sup> imine bond,<sup>11,12</sup> disulfide bond,<sup>7,13</sup> and Diels-Alder (DA) reaction.<sup>14,15</sup> Non-

<sup>†</sup>To whom correspondence should be addressed.  
hx0029@gyu.edu.cn, ORCID<sup>®</sup>0000-0002-1444-576X  
©2022 The Polymer Society of Korea. All rights reserved.

covalent bonds such as hydrogen bond,<sup>16,17</sup>  $\pi$ - $\pi$  stacking,<sup>18,19</sup> ionic interactions<sup>20,21</sup> are also frequently used to fabricate self-healing polymers. However, only paying attention to the self-healing abilities of as-prepared self-healing polymers and ignoring their mechanical performances will inevitably narrow the application fields of them. Therefore, huge impetus was ignited to prepare novel self-healing polymers with admirable mechanical properties. Unfortunately, favorable self-healing ability and novel mechanical properties are a perpetual conflict, because factors that benefits of self-healing are usually detrimental to the mechanical properties. For instance, high chain mobility is agreeable to self-healing, but it is a formidable obstacle to improve the strength of the polymers.<sup>16,22,23</sup>

Polyurethane (PU), in its chemical structure, consists of soft segment with relatively high chain mobility and low glass transition temperature ( $T_g$ ), and hard segment with rigid chain structure and high  $T_g$ .<sup>7,8,24,25</sup> Moreover, the two segments are thermodynamical incompatible, and they are in a state of microphase separation. The chemical structure particularity makes PU become a potential candidate for assembling an excellent self-healing polymer with satisfactory machinal properties via adjusting the ratio of the soft and hard segments. In addition, PU has unique advantage of molecular design flexibility due to varieties of the diisocyanates, polyols, and short chain extenders.<sup>26,27</sup> Ying and co-workers ingeniously proposed a fast room temperature self-healing PU with tensile strength as high as 9.8 MPa by using hydrophobic hydroxyl-terminated polybutadiene as the soft segment and the bis(4-hydroxyphenyl)disulfide as the chain extender.<sup>7</sup> However, the disulfide is a toxic chemical, which is both harmful to environment and human being.<sup>28</sup> Some academics innovatively balanced the self-healability and mechanical properties by "regulating phase" strategy, including cautious choosing the types of the hard segments and reasonable controlling the contents of the hard segments.<sup>22</sup> Another enlightening research disclosed a room-temperature self-healing PU with tensile strength and toughness up to 14.8 MPa and 87.0 MJ m<sup>-3</sup> respectively, and in their work, they adopted a strategy named "synergetic triple dynamic bonds", in which three kinds of dynamic bonds, reversible dimethylglyoxime-urethane (DOU) bond, Cu-DOU coordination bonds, and hydrogen bonds, together endowed the as-prepared PU with conspicuous mechanical robustness and highly desirable self-healing efficiency.<sup>29</sup> In spite of the successful use of dynamic bonds, the use of copper ions, a toxic raw material,<sup>30,31</sup> extremely reduced the impetus for practical applications of their research. As it is

shown, although so many outstanding achievements have been made, PU with attractive mechanical strength ( $\geq 15$  MPa) and strong self-healing ability is still in a relatively barren state, due to the intrinsic contradiction between chain rigidity for high mechanical strength and chain mobility for efficient self-healing ability. Generally speaking, self-healing PUs possess robust mechanical properties, especially the tensile strength, are highly valuable for applications in the fields such as resilient protection material for human being, anti-puncture tire, *etc.* Therefore, it is imperative to develop self-healing PUs owning distinguished healing efficiency as well as high tensile strength. Besides the mechanical performances, as higher requirements proposed, various kinds of polyurethanes have been developed, such as excellent thermal stability, ultraviolet (UV) blocking, *etc.* Among these functionalities, the UV blocking attracts the research interest of the researchers, because the UV radiation can lead to a myriad of adverse effects on human health and biological systems.<sup>32</sup> However, to dissipate the harmful energy from UV, self-colored chain extenders are often applied to synthesize the polyurethanes, which impairs the colorless of the polyurethane. For example, Zhang *et al.* reported a series of UV-absorbing polyurethane films by using curcumin as a chain extender.<sup>33</sup> Unfortunately, owing to yellow-colored chain extender (curcumin), the appearances of these obtained PU films are yellow, and especially the WPU-3, it is a dark yellow-colored film, which destroy the colorlessness and transparency of traditional polyurethane simultaneously. Zhou *et al.* described a self-healing polyurethane with admirable UV blocking property by introducing disulfide bonds and octadecane loaded titanium dioxide nanocapsules (OTNs)-graphene.<sup>34</sup> However, as mentioned above the disulfide is a toxic chemical, and to evenly disperse OTNs-graphene in polyurethane is another tedious and laborious work.

Herein, based on innovative and discreet selection of the diisocyanates and chain extender, we present a series of PUs that successfully combines excellent self-healability and mechanical properties at the same time, and meantime the advantages such as colorlessness and transparency of the polyurethane are preserved as well. The core of this work is regulating the supramolecular forces (H-bonds and  $\pi$ - $\pi$  interactions) through rational utilization of the hard segments and reasonable arrangement of the hard segment contents. Specifically, self-healing PUs (PUT-0, PUT-3, PUT-5, and PUT-10) were synthesized via two-step polyaddition reaction using polytetramethylene ether glycol (PTMEG) as the soft segment,

using isophorone diisocyanate (IPDI) and/or toluene diisocyanate (TDI) as the hard segments, and using 1,4-benzenedimethanol (BMO), as the chain extender, which contains benzene ring in its chemical structure, and therefore, it could offer extra  $\pi$ - $\pi$  interactions with TDI. Moreover, the BMO is a fine white crystal, and unlike the curcumin, the BMO can effectively avoid dyeing the obtained PU films. We expect that the optimum type and content of the hard segment can endow PU with excellent self-healing characteristics while maintaining its good mechanical properties. Among these as-prepared PUs, PUT-5 was chosen as the matrix, liquid metal as the filler, we prepared a demo of self-repairing wires. Moreover, with help of the Eu[(DBM)<sub>3</sub>EA]phen, we also proposed the potential application of the PUT in anti-counterfeiting materials.

## Experimental

**Materials.** Polytetramethylene ether glycol (PTMEG,  $M_n \approx 1000$ ) was purchased from Aladdin Chemical Reagent Co. (Shanghai, China), and the PTMEG was dried at 120 °C under vacuum for 2 h in advance. Isophorone isocyanate (IPDI), 1,4-benzenedimethanol (BMO), dibutyltin dilaurate (DBTDL), toluene diisocyanate (TDI), methyl orange, Victoria blue, and calcium hydride were provided by Shanghai Macklin Biochemical Co., Ltd, and they were used as received. Toluene, chloroform, tetrahydrofuran (THF), and *N,N*-dimethylformamide (DMF) were purchased from Sinopharm Chemical Reagent Co., Ltd. (Shanghai, China), and used after drying with calcium hydride. Liquid metal (Gallium-Indium-Tin alloy, melting point: 16 °C) and fluorescent powder (Eu[(DBM)<sub>3</sub>EA]phen) were purchased from the Beijing Hualide Technology Co., Ltd. Normal saline was obtained from Guangdong Huankai Microbial Technology Co., Ltd.

**Synthesis of PUT-x.** 12.5 g (12.5 mmol) of freshly dried PTMEG, 3.92 g of TDI (22.5 mmol), 11.66 g of IPDI (52.5 mmol), a drop of DBTDL and 50 mL of freshly dried toluene were firstly reacted at 80 °C in a 500 mL round three-necked flask equipped with a mechanical stirrer, an inlet for high purity nitrogen gas, and a condenser. 2 h later, a certain amount of BMO was charged into the flask, followed by stirring at 80 °C for another 2 h. The crude product was precipitated in excess of methanol several times, followed by drying at 45 °C in a vacuum oven for 8 h to constant weight. The molar ratios of the TDI to IPDI were systematically varied from 0:10, 3:7, 5:5, and 10:0, and accordingly, the obtained self-healing PUs were marked as PUT-0, PUT-3, PUT-5, and PUT-10.

**Preparation of PU Membranes.** Weigh a certain amount of thoroughly dried PUT-*x*, and dissolve it in THF to prepare solutions with fixed concentration of 30 wt%. Then, the PUT solutions were poured into a rectangular Teflon mold with dimensions of 110 mm×110 mm×5 mm. The solution was firstly placed at room temperature overnight, and then it was dried in a vacuum oven at 60 °C for 8 h and 80 °C for 2 h. Transparent and flat PU membranes was obtained.

**Fabrication of Self-healing Conductive Wire.** 30 wt% of liquid metal was directly mixed with the 70 wt% of PUT-5 solution to obtain a mushy composite. Further, the mushy composite was dried in a vacuum oven at 60 °C for 8 h and 80 °C for 2 h to obtain the self-healing conductive wire.

**Preparation of Fluorescent Anti-counterfeiting PU Film.** Similar to the preparation of self-repairing wires, 0.1 g of Eu[(DBM)<sub>3</sub>EA]phen was firstly dissolved in 10 mL of chloroform, and then the obtained solution was added into 10 mL of PUT-5 solution (30 wt%). Further, the mixed solution was dried in a vacuum oven at 60 °C for 8 h and 80 °C for 2 h. A light yellow and transparent anti-counterfeiting PUT film was prepared.

**Characterizations.** The <sup>1</sup>H NMR and <sup>13</sup>C NMR spectra for chemical structure confirmation were performed on a Bruker AVANCE III 400 MHz at room temperature in CDCl<sub>3</sub> using tetramethylsilane (TMS) as the internal standard. Fourier transform infrared spectra (FTIR) were performed on a Thermo is50 using attenuated total reflectance (ATR) mode. The spectra were collected from 4000 to 400 cm<sup>-1</sup> with 32 scans at a resolution of 4 cm<sup>-1</sup> at room temperature. Moreover, to test the H-bonds, temperature variable FT-IR was recorded on an iD5 ZnSe ATR instrument, and the data were collected after holding the temperature at the desired temperature for 30 min.  $T_g$  of as-prepared PUs were record on a NETZSCH DSC 214 under a nitrogen atmosphere. Around 3.00 mg of each sample was sealed in a 40  $\mu$ L aluminum crucible, and before recording the  $T_g$ , all samples were heated to 150 °C and kept for 3 min to eliminate the thermal histories. Dynamic thermomechanical analysis (DMA) was performed on a TA Instruments DMA Q800. The measurements were carried out with a Multi-Frequency-Strain operator at a frequency of 1 Hz with the amplitude of 2  $\mu$ m, and the data were collected from -110 to 150 °C at a heating rate of 3 °C min<sup>-1</sup> in a liquid nitrogen atmosphere. Thermogravimetric analysis (TGA) was conducted on a NETZSCH TG209F1 thermogravimetric analyzer under nitrogen atmosphere. To evaluate the thermal stabilities of the PUs, around 8 mg of the PUT was charged into an 80  $\mu$ L corundum

crucible and heated from 50 to 800 °C with a fixed heating rate of 20 °C min<sup>-1</sup>. Tensile tests were carried out on an Instron 3365 machine with a stretching rate of 50 mm·min<sup>-1</sup> at room temperature. The samples were prepared as dumb-bell shape, and the geometric dimensions were 10 mm×2 mm×1.5 mm (length×width×thickness) for each sample. For each sample, at least three splines were tested, and the tensile strength is taken the average value of the splines. Before testing, each sample was pretreated at a temperature of 25 °C and a humidity of 50% for 48 h. In order to test the self-healing properties of as-prepared PUs, the dumbbell-shaped spline was completely cut into two sections at the middle point of the spline. After healing at varied temperatures and times, the mechanical properties of the self-healed splines were measured by Instron 3365, and the self-heal efficiency was evaluated by the ratio of the tensile strength of healed spline over the corresponding tensile strength of the original one (eq. (1)):

$$\text{Self-healing efficiency (\%)} = \frac{\text{Tensile strength of the self-healed PUT-}x}{\text{Tensile strength of the original PUT-}x} \quad (1)$$

where the tensile strength of the original PUT-*x*, tensile strength of the self-healed PUT-*x* are the average value of the original splines and self-healed splines, respectively.

The scratch recovery was observed on an Olympus/BX 51TF Instec H601 optical microscope which equipped with a hot stage. To conduct the ultraviolet-visible (UV-Visible) transmittance experiment, the PU films were cut into square flake with dimensions of 2.5 mm×2.5 mm (length×width), and the data were collected on a Hitachi U3900 spectrophotometer at room temperature. The ultraviolet-visible (UV-vis) spectra

were recorded on a computer-controlled ThermoFisher Scientific Evolution 350 spectrophotometer, using THF as a reference solvent. The scanned area was from 200 to 1100 nm.

## Results and Discussion

**Synthesis and Characterization of the Self-healing Polyurethanes (PUT-*x*).** According to Ying *et al.*, the PUs obtained *via* two-step method demonstrates the feature of admired chain length distribution of the hard segments.<sup>7</sup> Thus, two-step protocol was also employed to synthesize the target PUT-*x* in this work.<sup>7,35</sup>

Detailedly, the polydiol (PTMEG) and the diisocyanate (IPDI and/or TDI) undergo polyaddition reaction at first to obtain prepolymers, and then desired linear PUT-*x* containing distinct contents of TDI were fabricated by reacting the chain extender (BMO) with corresponding prepolymers (Figure 1(a)).<sup>36</sup> Note that, in PUT-*x* systems, two types of diisocyanates (TDI and/or IPDI) were selected as the hard segments, while the IPDI bestows high transparency and superior mechanical property on the obtained PUT-*x*, the TDI endows the PUT-*x* with more benzene rings in the molecular chain, which are the active sites for  $\pi$ - $\pi$  stacking (Figure 1(b)).<sup>37,38</sup> Besides, the aromatic chemical structure of BMO can also facilitate the  $\pi$ - $\pi$  interactions of the PUT-*x*. The specific feeding parameters, hard segment contents and mass percentages of the IPDI and TDI are summarized in Table S1 and S2 (Supporting Information).

The successful synthesis of PUT-*x* was firstly investigated by nuclear magnetic resonance (NMR). Two singlet resonances with nearly equal integration values in range of 9.1 to 9.8 ppm, corresponding to the protons of Ar-NH-C in the urethane

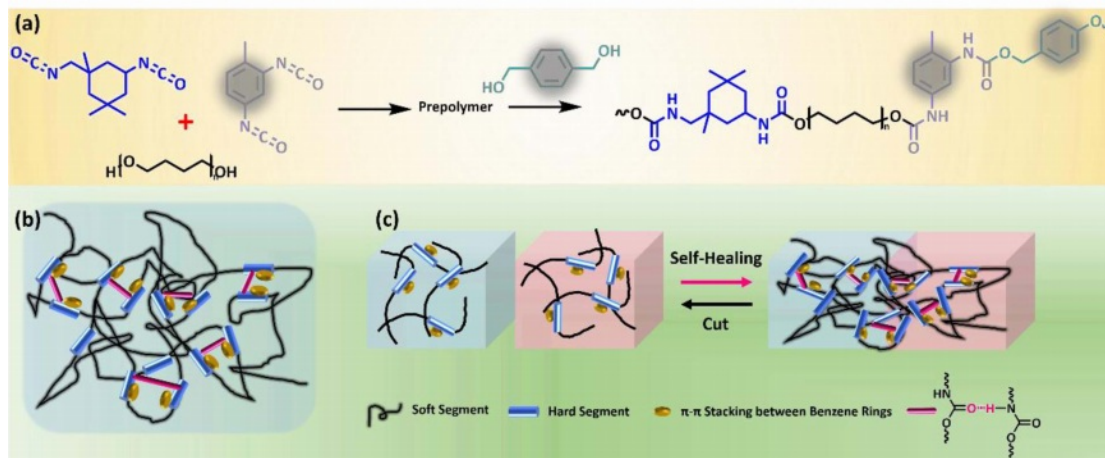


**Figure 1.** Chemical structure design of the self-healing polyurethanes (PUT-*x*): (a) schematic illustration of synthetic routes of PUT-*x*; (b) ideal chain structure of the PUT-*x* that composed of soft segments and hard segments; (c) cut and self-healing process of the PUT-*x*.

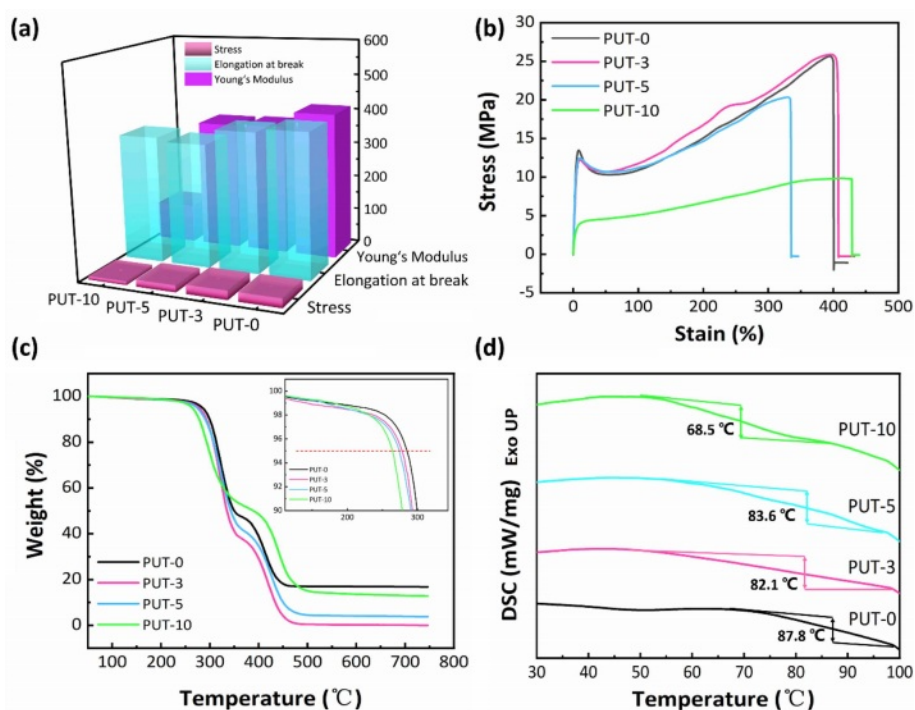


**Figure 2.** Thermomechanical properties of the self-healing polyurethanes (PUT-*x*): (a) the calculated average values of the tensile stress, elongation at break, and Young's modulus; (b) representative stress vs. strain curves; (c) TGA curves obtained under a nitrogen atmosphere; (d) DSC curves collected from the second heating cycle.

group (Figure S1).<sup>39</sup> Furthermore, the polymerization of the PUT-*x* has also been clearly demonstrated by the disappearance of the characteristic peak of the -NCO group, which locates at  $2264\text{ cm}^{-1}$  (Figure S2).<sup>8,40-43</sup> Moreover, the peaks center at around  $1710$  and  $1250\text{ cm}^{-1}$  correspond to the stretching vibrations of C=O and C-O groups in PUT-*x*.<sup>44,45</sup> The band displays at  $3310\text{ cm}^{-1}$  is assigned to the stretching vibration of the N-H group,<sup>46</sup> and the band at  $1590\text{ cm}^{-1}$  corresponds to the skeleton vibration of the benzene rings.<sup>47</sup> What surprised us most is that with the addition of TDI, a newly emerging peak representing the H bonds between the N-H and C=O appears at around  $1675\text{ cm}^{-1}$ , and the new peak confirms the C=O group involves the formation of the H bonds explicitly.<sup>46</sup> Moreover, the intensity of the new peak gradually increases along with the increase of the TDI contents in PUT-*x*, indi-

cating that as the amount of the TDI increases, more and more C=O groups engage in forming the H bonds with N-H groups.

**Mechanical Properties of PPU Elastomers.** Preminent mechanical property is the key factor for fabrication useful devices, and the mechanical performances of pretreated PUT-*x* splines were evaluated by uniaxial tensile tests at a speed of  $50\text{ mm min}^{-1}$  under ambient condition. The average values of the tensile stress, elongation at break, and Young's modulus are shown in Figure 2(a), and the more detailed and concrete data are summarized in Table 1.

The samples demonstrate tensile strength in the range of 10 to 26 MPa (Table 1). Presumably, the tensile strength of the PUT-*x* increases with the increase of the TDI content, because the TDI contains the benzene ring, which is a rigid chemical structure.<sup>48</sup> Unfortunately, the result is exactly opposite to our

**Table 1. Mechanical and Thermal Parameters of the PUT-*x***

Samples	Tensile Strength (MPa)	Young's Modulus (MPa)	Elongation at break (%)	$T_g$ (DSC °C)	$T_g$ (DMA °C)	$T_{d\ 5\%}$ (°C)	$R_{750\ ^\circ\text{C}}$ (%)
PUT-0	26.3±0.8	412.8±1.1	405.3±8.5	87.8	82.3	284.6	16.8
PUT-3	26.1±1.3	368.8±0.5	410.9±5.7	82.1	80.9	278.1	0.3
PUT-5	19.9±0.4	366.4±0.2	337.1±4.2	83.6	79.7	273.9	3.7
PUT-10	8.7±1.8	109.2±0.6	418.5±6.2	68.5	66.8	264.2	12.8

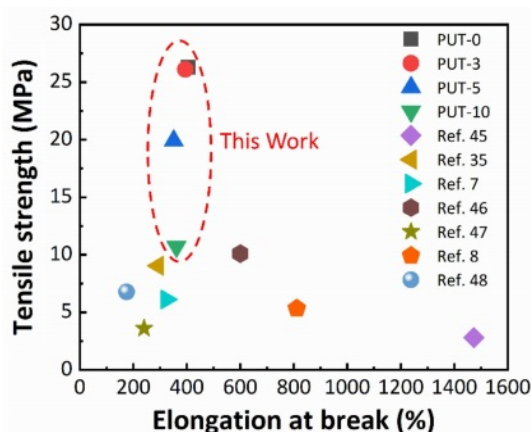


**Figure 3.** Comparison of tensile stress between this work and other self-healing polyurethanes. Note: Some tensile stress data were estimated according to the strain-stress curves published on the reference.

forecast, and we attribute this phenomenon to the fact that the TDI used in this work was the mixture of 2,4-tolylene diisocyanate and 2,6-tolylene diisocyanate, which impairs the regularity of the molecular chain, therefore, the crystalline properties and tensile stress of the polyurethane are weakened.<sup>49</sup> Note that, even with highest content of TDI (PUT-10) among PUT-*x*, it demonstrates an impressive tensile strength of 10.7 MPa (Figure 2(b)), which is larger than the tensile strength of many reported self-healing polyurethanes (Figure 3),<sup>7,8,40,50-53</sup> the PUT-5 shows a remarkable tensile strength of almost up to 20 MPa and an elongation larger than 350% (Figure 2(b)).

Thermal stability is another valuable parameter to evaluate the potential practical applications of PUT-*x*. TGA was utilized to assess the thermal stabilities of the PUT-*x*, and as it is shown that all of the PUT-*x* exhibit outstanding thermal stabilities, with the  $T_{d5\%}$  higher than 260 °C, even higher than that of the cross-linked self-healing PU<sup>40</sup> or PU with dynamic oxime-car-

bamate bonds.<sup>54</sup> Moreover, TGA measurement also discloses the PUT-*x* have two stages of thermal decomposition (Figure S3), in which the first stage degradation ( $T_{5\%}$ ) starts in range of 265 to 285 °C (Figure 2(c)), probably due to the degradation of the urethane bonds and decomposition of the soft segments.<sup>55</sup> The second stage of decomposition above 400 °C corresponds to the cleavage of the hard segments.<sup>56</sup> Although the char yields of PUT-0 and PUT-10 at 750 °C ( $R_{750^\circ\text{C}}$ ) are all higher than 5% (Figure 2(c)), demonstrating relatively good thermal stability, the char yields of the PUT-3, PUT-5, and PUT-10 are lower than that of the PUT-0, and the result can be attributed to the decrease of the hard segment contents (Table S2). In addition, the thermal behaviors of PUT-*x* was further investigated by DSC, as shown in Figure 2(d). The  $T_g$  values are about 87.8, 82.1, 83.6, and 68.5 °C for PUT-0, PUT-3, PUT-5, and PUT-10, respectively. As it is shown the  $T_g$  values of all PUT-*x* are much higher than room temperature, which ensures that all PUT materials can exhibit excellent mechanical performances at room temperature.

The DMA was further employed to characterize the dynamic thermal-mechanical behaviors of PUT-*x*, as shown in Figure 4.

As can be seen, only one-step decrease of storage modulus was discerned for all PUT-*x* systems when the temperature increased from -100 °C to 125 °C (Figure 4(a)). Moreover, the values of storage modulus for PUT-*x* are higher than 1.1 GPa at room temperature, which also corroborates the results obtained from the DSC test that all PUT-*x* feature good mechanical properties at room temperature. The  $T_g$  of PUT-*x* were determined by the peak temperatures in Figure 4(b), which were 82.3, 80.9, 77.7, and 66.8 °C, respectively. As displayed, the  $T_g$  gradually decreased along with the decrease of the hard segment content, indicating that the  $T_g$  is greatly affected by the hard segment content, and it seems that the

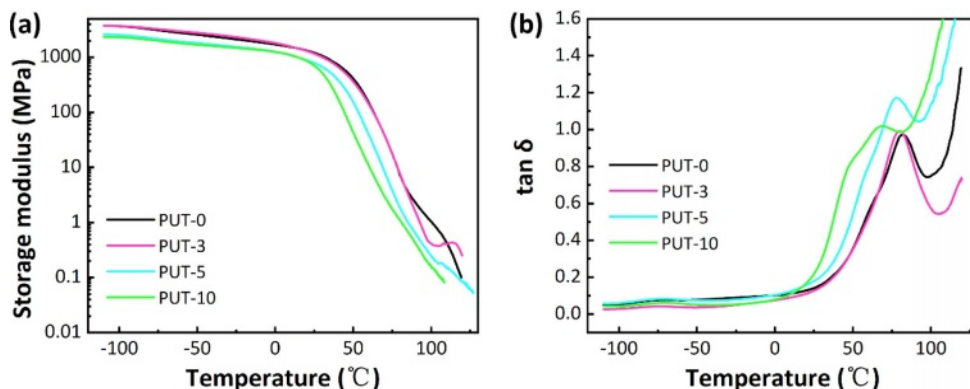


**Figure 4.** Dynamic thermal-mechanical analysis of PUT-*x*: (a) the storage modulus curves of PUT-*x* vs. temperature; (b) the loss factor curves of PUT-*x* vs. temperature.

content of TDI or IPDI has obscure effect on  $T_g$  of the PUT- $x$ . The  $T_g$  obtained from DMA tests display obscure differences from the results measured by DSC owing to different experimental methods.<sup>57</sup> Note that, larger and more conspicuous peaks can be distinguished at temperature higher than 80 °C, and we attribute these peaks to the melting process of the PUT- $x$ .<sup>58</sup>

**Self-healing Performances of PUT- $x$ .** All the PUT- $x$  film are transparent, especially the PUT-0, PUT-3, and PUT-5 are colorless, and only the PUT-10, with the highest content of TDI among PUT- $x$ , displays yellow color appearance slightly (Figure S4). To further inspect the transmittance, absorbance, and reflection properties of the PUT- $x$  films, all PUT- $x$  were cut into square samples with dimensions of 2.5 cm×2.5 cm×1 mm (length×width×thickness), and the samples were investigated by a UV-Visible spectrophotometer (Figure 5(a), Figure S5). Noticeably, all samples with transmittance in the range of 400 to 800 nm are greater than 80% (Figure 5(a) solid lines), and the reflection of them are all about 10% (Figure S5). Both the results of digital images and UV-Visible test demonstrate that the PUT- $x$  display high visible light transmittance and acceptable colorlessness, which benefit from the asymmetrical

chemical structure of IPDI.<sup>59</sup> Even more, the TDI employed in this work is not a pure TDI but a mixture of 2,4-tolylene diisocyanate and 2,6-tolylene diisocyanate, which can effectively reduce the regularity of the molecular chain, could significantly facilitate the transparency of the PUT- $x$  films.<sup>60</sup> Moreover, it seems that the addition of the TDI will enhance the reflectivity to the visible light of the PUT- $x$ , since the reflection in range of 400-800 nm gradually increases in the order of PUT-0, PUT-3, PUT-5, and PUT-10 (Figure S5).

What indeed surprised us most is the fact that all films exhibit impressive ability for absorbing the ultraviolet rays in range of 200 to 400 nm (Figure 5(a), dotted lines). Moreover, the absorption of the ultraviolet rays increases along with the increase of the TDI contents, and especially, the PUT-5 and PUT-10 can effectively absorb more than 80% of ultraviolet rays, which may correspond with the higher contents of the benzene rings of them in PUT- $x$ .<sup>61</sup> This feature allows PUT- $x$ , especially the PUT-5 and PUT-10, to protect the human from ultraviolet rays when they are used as electronic skins.<sup>7</sup>

In order to express the self-healing behaviors of the obtained PUT- $x$  in a more intuitive and explicit manner, two PUT-5 splines were dyed red and blue with methyl orange and Vic-

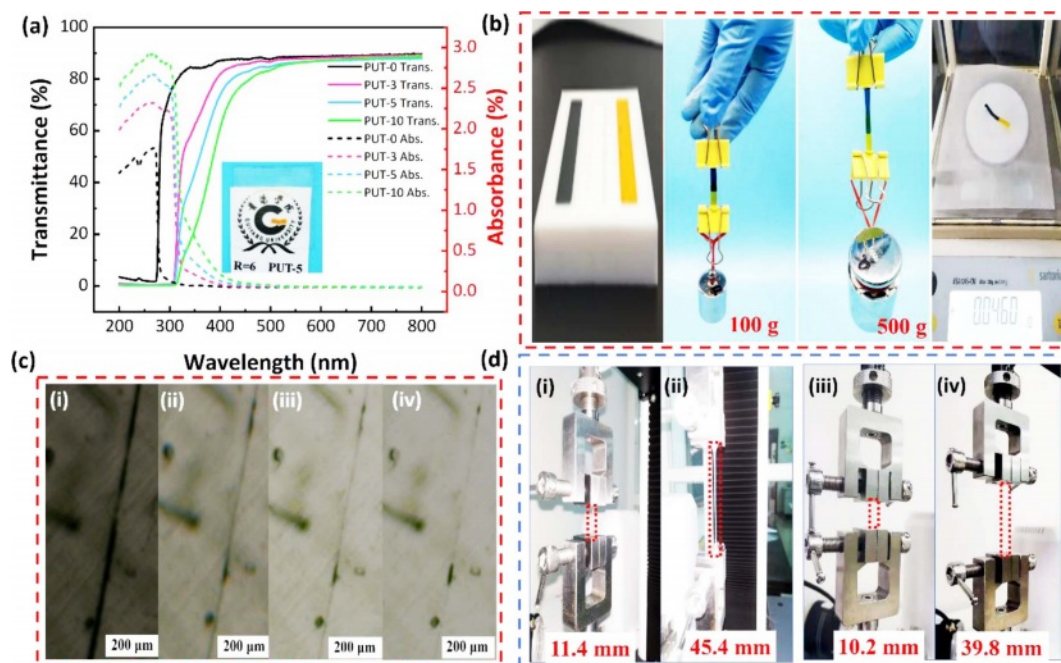


**Figure 5.** Appearance and self-healing performances of the PUT- $x$ : (a) UV-vis transmittance and absorbance spectra of PUT- $x$  films in the range of 200-800 nm, inset displays the image of the PUT-5 film to show the transparency of the PUT- $x$ ; (b) digital images of two pieces of dyed PUT-5 samples (one is dyed with methyl orange, the other one is dyed with Victoria blue), heated at 80 °C for 1 h, and then the healed sample was loaded for 100 g and 500 g counterpoises, respectively; (c) optical microscopic images of healing process for a scratch in PUT-5 at 80 °C for healing (i) 0 min, (ii) 10 min, (iii) 20 min, (iv) 30 min; (d) digital images of the tensile tests of scratched PUT-5 after being healed at 80 °C for 30 min: the first cycle (i and ii) and the second cycle (iii and iv).

toria blue respectively, and the two splines were healed at 80 °C for 1 h. The healed spline can load a 100 g counterpoise without any deformation, and moreover, when loaded with a 500 g counterpoise, the healed spline only shows a bit of deformation, and no tear has been identified, demonstrating the astonishing ratio (higher than 10000) of load to mass of PUT-5 (Figure 5(b)). Except for complete tear, scratch is a kind of more common damage to materials, and considering the situation, all the PUT-*x* were cut in the middle part with a scalpel, followed by the observation of their self-healing processes toward scratches with an optical microscope equipped with a hot stage (Figure 5(c), Figure S6-S8). Taking PUT-5 as an example, its self-healing process toward scratch at 80 °C is display in Figure 5(c). As it is shown, initially, the scratch can be identified as an obvious dark line under the microscope, and 10 min later, the dark line fades evidently and almost disappeared after 30 min (Figure 5(c)). Furthermore, addition of the TDI to the molecular chain evidently facilitate the self-healing process of the PUT-*x* system, especially the PUT-10, it self-healed the scratch at 80 °C in only 3 min (Figure S8). Due to two factors that the TDI can effectively promote the self-healing process of PUT-*x* system: one is that compared with IPDI, TDI can introduce more benzene rings into the molecular chain of the

PUT-*x* system, and thus, more aromatic  $\pi$ - $\pi$  interactions effectively are generated between TDI and BMO segments,<sup>62</sup> the other one is that the TDI used in this work is a mixture of 2,4-tolylene diisocyanate and 2,6-tolylene diisocyanate, as mentioned above, which can enhance the chain mobility by impairing the chain regularity.<sup>7</sup> Moreover, to further scrutinize the crack initiation of the scratch healed specimens at 80 °C for 30 min, tensile test was employed to record the maximum length at which a crack can be identified by naked eyes (Figure 5(d)). For PUT-0, visible crack appeared near the healed scratch when the elongation reached 19.1% (Figure S9), and as for PUT-3, PUT-5, and PUT-10, the visible cracks emerged at elongations of 217.9% (Figure S10), 298.2% (Figure 5(d) first cycle), and 365.4% (Figure S11) respectively. The results of the crack initiation of the scratch healed specimens clearly demonstrate that the TDI accelerate the self-heal process of the PUT-*x* system effectively because of the extra  $\pi$ - $\pi$  interactions produced by TDI.

To better understand the influences of healing temperatures and healing time periods on self-healing efficiency, thoroughly scissored PUT-*x* specimens were self-healed at varied temperatures for different time periods, and then tensile tests were conducted at a fixed speed of 50 mm min<sup>-1</sup> on the healed spec-

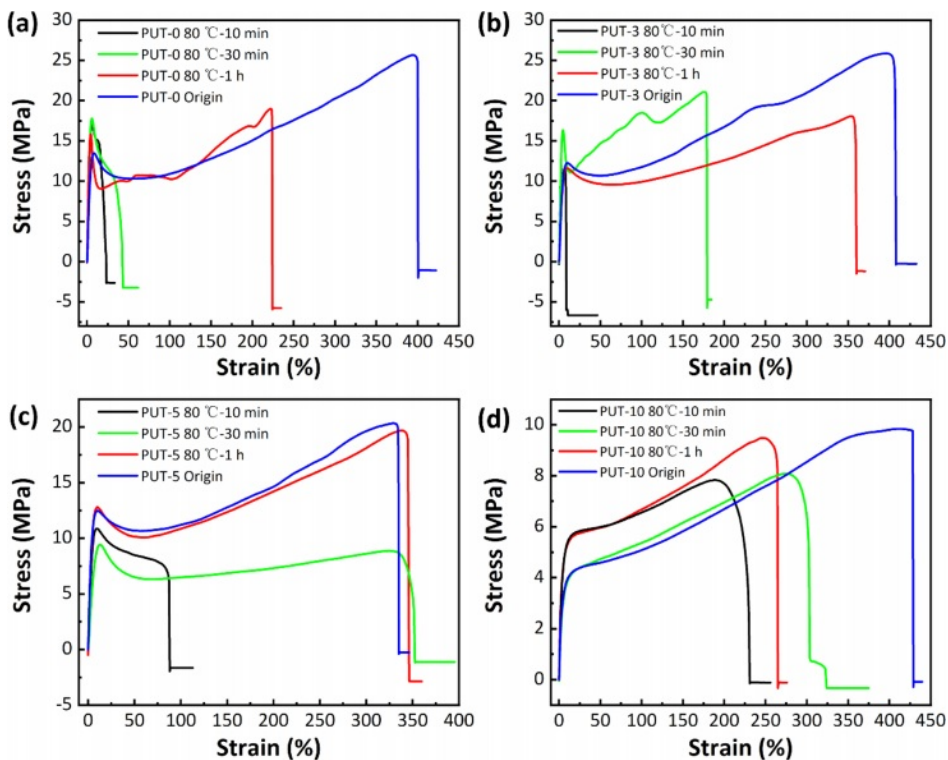


**Figure 6.** Strain vs. stress curves of scissored PUT-*x* specimens self-healed at 80 °C with different time intervals: (a) PUT-0; (b) PUT-3; (c) PUT-5; (d) PUT-10.

imens to characterize their mechanical performances. As presented, stress-strain curves of the healed specimens again illustrate the TDI promotes the self-healing behaviors of the PUT-x because under the same self-heal temperature and time period, the polyurethanes containing TDI (PUT-0, PUT-3, and PUT-10) show larger values of tensile strength and elongation than the PUT-0 (Figure 6, Figure S12 and S13). Noticeably, the recovered mechanical properties of PUT-5 were already comparable to its original properties after it was self-healed at 80 °C for 1 h (Figure 6(c)). Moreover, as expected and reported, lower self-healing temperature leads to reduction of self-healing efficiency, but such disadvantage can be compensated by extending the self-healing time (Figure S12 and S13).<sup>50</sup> To further obtain the quantitative data of the self-healing behaviors, self-healing efficiencies were calculated by eq. (1) and presented in Figure 7. As shown, either under the same self-healing temperature or same self-healing time period, the specimens contain TDI show higher self-heal efficiency than the ones contain no TDI at all, and the results are consistent with the results obtained from their self-healing processes of scratches (Figure 5(c)).

**H-bonds and  $\pi$ - $\pi$  Stacking Characterization.** To explain the self-healing behaviors of the PUT-x from the perspective of molecular mechanism, the *in-situ* FTIR was used to study the dependence of the H-bonds on temperature.<sup>63</sup> Three typical samples (PUT-0, PUT-5, and PUT-10) were carefully selected to implement the temperature-dependent FTIR analysis (Fig-

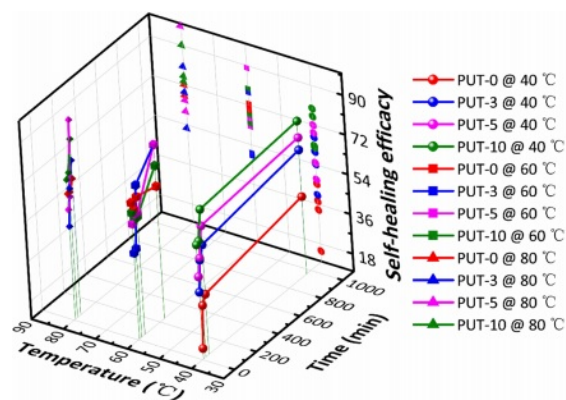


**Figure 7.** 3D representation of the self-healing efficacy of PU-x system at varied temperatures and time periods.

ure S14), and moreover, the main characteristic bands correspond to the H-bonded C=O and free C=O groups are magnified and shown in Figure 8. As it is shown, the typical temperature variation FTIR spectrum of PUT-0 clearly demonstrates the peak shift and area change during heating (Figure 8(a)). In contrast, for PUT-5 and PUT-10, no evident peak shift can be recognized during the heating process, except for the slight reduction of the peak area (Figure 8(b) and 8(c)). This is highly related to the chemical structures of the PUT-5 and PUT-10, which contain more benzene rings than the PUT-0 due to the addition of TDI. The short-range ordered rigid aromatic TDI endows the obtained polyurethanes with stable and strong intermolecular and intramolecular interactions.<sup>38</sup> Sub-

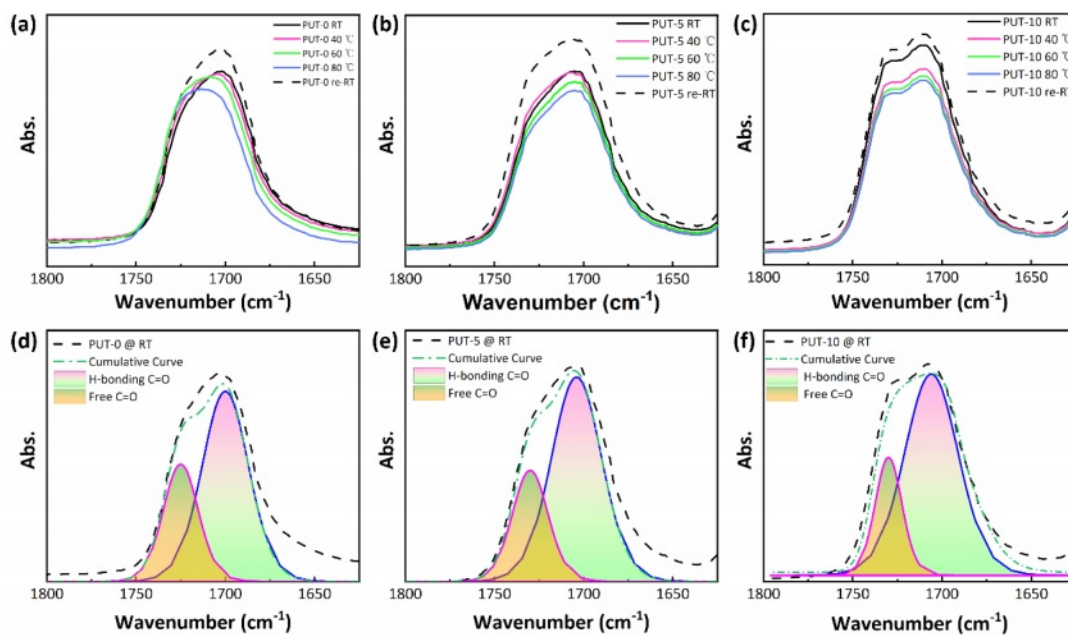


**Figure 8.** temperature-dependent FTIR spectra of the C=O regions: (a) PUT-0; (b) PUT-5; (c) PUT-10; the H-bonded and free C=O groups of (d) PUT-0; (e) PUT-5; (f) PUT-10.

sequently, we performed a curve fitting of the carbonyl group vibration region (1650-1800  $\text{cm}^{-1}$ ) using a Gaussian-Loren-Cross function, and two individual peaks were resolved. The peaks centers at around 1700  $\text{cm}^{-1}$  are assigned to stretch vibration of the H-bonded C=O, and the peaks locate at 1725  $\text{cm}^{-1}$  corresponds to stretch vibration of the free C=O (Figure 8(d), 8(e) and 8(f)).<sup>7,64</sup> The percentage of the H-bonded C=O was calculated by eq. (2),<sup>7</sup> and the data were summarized in Table S3.

$$\text{H-bonded C=O (\%)} = \frac{A_{1700}}{A_{1700} + A_{1725}} \times 100\% \quad (2)$$

where  $A_{1700}$  and  $A_{1725}$  are the fitted peak areas at 1700 and 1725  $\text{cm}^{-1}$ . 68.26, 72.02 and 77.33 percent of H-bonded carbonyl groups apparently illustrate that most of the carbonyl groups of the PUT- $x$  have formed hydrogen bonds at room temperature.

In addition to H-bonds,  $\pi$ - $\pi$  stacking is also a nonnegligible aspect between the short-range ordered aromatic ring structures in aromatic polyurethane.<sup>38,65</sup> Due to the addition of the TDI, the PUT-3, PUT-5 and PUT-10 contain more aromatic ring structures than the PUT-0, and consequently, we speculate that the  $\pi$ - $\pi$  stacking effects in PUT-3, PUT-5 and PUT-10 are stronger than that in the PUT-0. In order to more intuitively test the  $\pi$ - $\pi$  stacking effect caused by the benzene rings, a series of PUT- $x$  solutions were prepared with mixture of toluene and tetrahydrofuran as the solvent (Figure 9).

We anticipate that  $\pi$ - $\pi$  stacking effects in the PUT- $x$  molecular chain would be partially transferred into the  $\pi$ - $\pi$  interactions between PUT- $x$  and the toluene. In these as-prepared solutions, the ratios of tetrahydrofuran and toluene in the mixed solvent were 0:10, 7:3, 6:4, 5:5, 4:6 and 3:7 respectively, and the concentration of PUT- $x$  in the solution was fixed at 10 wt%. It can be seen that all PUT- $x$  can be completely dissolved, when the solvent is tetrahydrofuran. In addition, as presented in Figure 9, PUT-0 can be perfectly dissolved, regardless of the content of the toluene in the mixed solvent. In contrast, when the content of toluene in the mixed solvent is high, (tetrahydrofuran: toluene=3:7) the solubilities of the PUT-3, PUT-5 and PUT-10 decrease in order, and especially for the PUT-10, when the content of toluene in the solvent is more than 50%, a gel is formed (Figure S15). Through this solubility experiment, we intuitively proved that introduction of TDI to the polyurethane molecular chain can effectively promote more  $\pi$ - $\pi$  interactions. In order to conduct an in-depth research about the influence of  $\pi$ - $\pi$  stacking of phenyl units on optical properties, UV-vis measurement was carried out for PUT- $x$  systems (Figure S16). In detail, the UV-vis absorption spectra of all

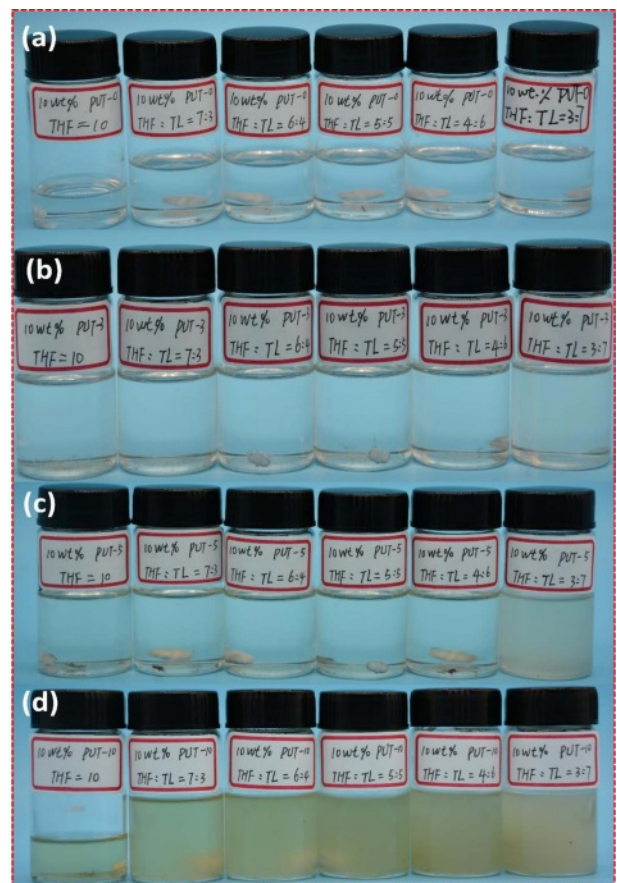


**Figure 9.** Solubility of the PUT- $x$  in mixed solvent of tetrahydrofuran (THF) and toluene (TL): (a) PUT-0; (b) PUT-3; (c) PUT-5; (d) PUT-10.

PUT- $x$  system exhibit broad adsorption band from 300 to 400 nm, which is consistent with those previously reported literature.<sup>66</sup> Although all PUT- $x$  demonstrate the characteristic peak of the  $\pi$ - $\pi$  stacking, the intensities of polyurethanes containing TDI (PUT-3, PUT-5 and PUT-10) are significantly stronger than that of the PUT-0. This is probably due to the fact that the addition of TDI makes the obtained polyurethanes develop a short-range ordered rigid aromatic structure in hard domains, which further results in strong  $\pi$ - $\pi$  interactions.<sup>38</sup> Oppositely, the PUT-0 contains no aromatic isocyanate (TDI), thus neither a short-range orderly aromatic structure nor strong  $\pi$ - $\pi$  interactions was formed in the PUT-0, which further extremely cripples the self-healing ability of the PUT-0.

**Potential Applications of Self-healing of PUT- $x$ .** Given their excellent integration of robust mechanical properties and decent self-healing abilities, the PUT- $x$  systems, especially the PUT-5, show the promising potentials for fabricating various self-healable devices. As a proof-of-concept demonstration, PUT-5 was chosen as the self-healable matrix to assemble a

conductive wire. Firstly, the PUT-5 was mixed with liquid metal at ratio of 50 wt% to 50 wt% and sonicated for 30 min to obtain a uniform and stable PUT-5/liquid metal sludge, and then the small amount of solvent in the sludge was completely removed by drying at 80 °C for 6 h in an oven. Subsequently, the conductive wire was connected to a circuit equipped with a blue light-emitting diode (LED) and batteries (Figure 10(a-

i)), and as expected the LED was turned on, indicating the satisfied conductivity of the PUT-5/liquid metal conductive wire. Note that according to Liang team, the transition from an insulator to excellent conductor, the conductivity should increase from nonconductive to  $1.89 \times 10^5 \text{ S cm}^{-1}$ .<sup>67</sup> Moreover, the LED went off when the conductor was cut into two pieces (Figure 10(a-ii)). Finally, the two detached wires were attached and

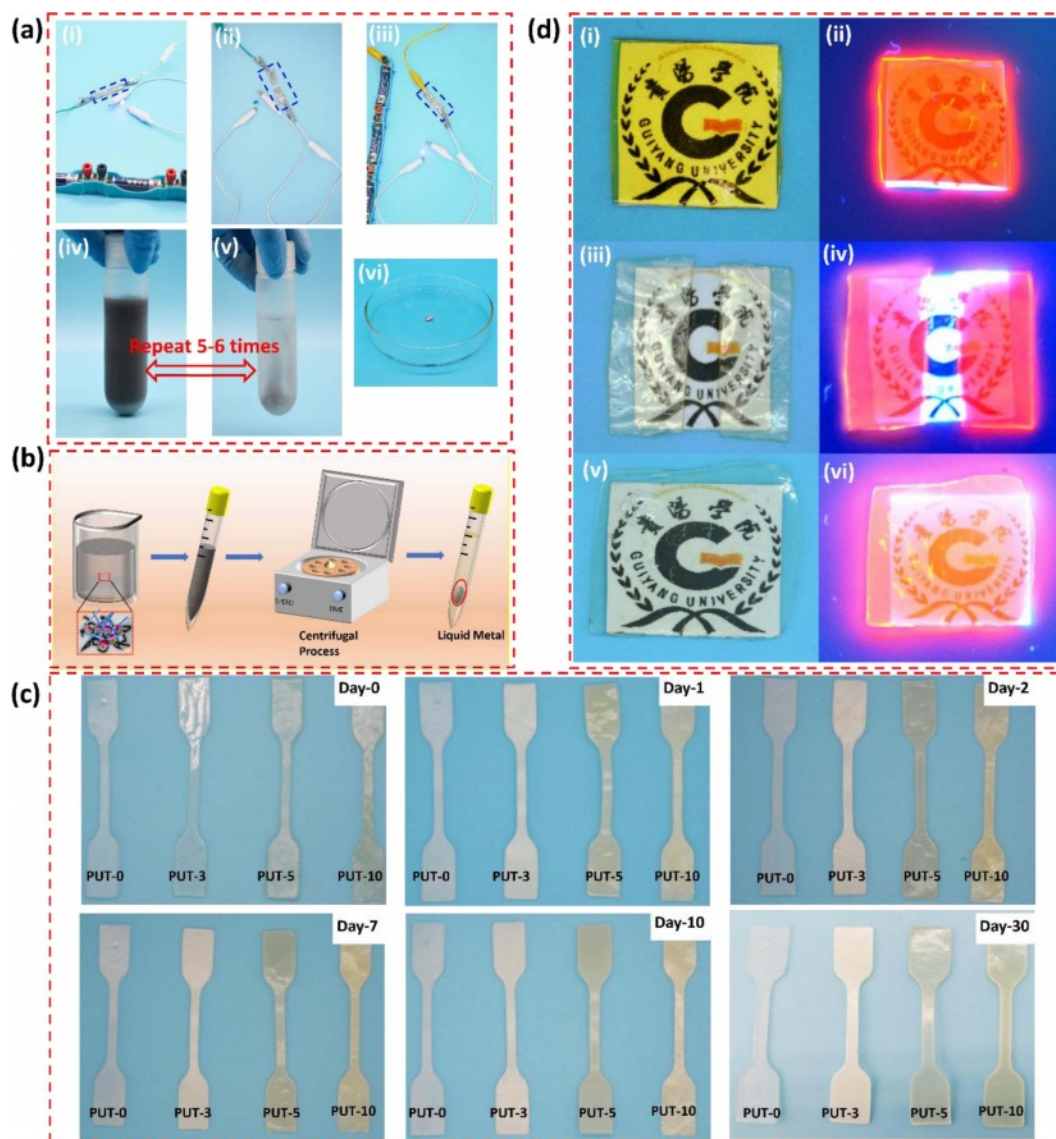


**Figure 10.** (a) digital images of the self-healable PUT-5/liquid metal conductive wire and recycle process of the liquid metal: (i) the LED was lit at the original stage; (ii) the conductive wire was cut; (iii) the scissored conductive wire was self-healed at 80 °C for 1 h; (iv) dissolution of PUT-5/liquid metal conductive wire by tetrahydrofuran; (v) the product after dissolving and washing for 5-6 times; (vi) recycled liquid metal; (b) schematic illustration of the recycling process of the liquid metal from the conductive wire; (c) digital images of PUT-*x* systems immersed in saline for varied time periods; (d) self-healable PUT-5 used as anti-counterfeiting material: (i) the PUT-5/Eu[(DBM)<sub>3</sub>EA]phen film at the original stage; (ii) the fluorescence of PUT-5/Eu[(DBM)<sub>3</sub>EA]phen film upon excitation at 365 nm; (iii) the scissored PUT-5/Eu[(DBM)<sub>3</sub>EA]phen film after storage at ambient condition for 30 days; (iv) fluorescence of PUT-5/Eu[(DBM)<sub>3</sub>EA]phen the scissored film; (v) the scissored PUT-5/Eu[(DBM)<sub>3</sub>EA]phen film was self-healed at 80 °C for 1 h; (vi) fluorescence of self-healed PUT-5/Eu[(DBM)<sub>3</sub>EA]phen film.

self-healed at 80 °C for 1 h, the LED was successfully lit again, clearly, the brightness after self-healing process almost equal to that before the self-healing, indicating the successful recovery of the conductivity (Figure 10(a-iii)).<sup>68</sup>

Moreover, it should be noted that not limited to conductivity and self-healing, both the PUT-5 and the liquid metal can be efficiently recycled from conductive wire, which perfectly solve the challenging problem of the waste disposal of organic-inorganic hybrid.<sup>69</sup> As displayed, the PUT-5 and liquid metal can be retrieved by dissolving and heating the conductive wire in THF at 80 °C for several times (Figure 10(a-iv) and 10(a-v)). By centrifugation, the liquid metal and the PUT-5 contained THF have been successfully separated (Figure 10(a-vi)), and in our work, the recycling efficiency was as high as 53.8 wt%. Although the retrieval rate is not as high as some reported literatures<sup>69,70</sup> the retrieval process of this work is easy and simple, only involves the dissolution and centrifugation (Figure 10(b)). Moreover, during the retrieval process, no strong acids or bases such as HCl, NaOH were used in our work, which tremendously reduce the possibility of secondary pollution.

To be used as self-healable substrate for human used devices, for example e-skin matrix,<sup>7,71</sup> the PUT-*x* should be able to withstand the corrosive effects of human sweat. However, polyurethane shows a certain degree of water absorption naturally due to the hydrophilicity of the urethane bonds,<sup>7,72</sup> which undermines the water resistance of polyurethane, let alone the resistance of human sweat. To evaluate human sweat resistance of the PUT-*x*, dumbbell-shaped specimens of PUT-*x* were immersed in normal saline, and their shapes and appearances were recorded at certain intervals (Figure 10(c)). As it is presented, the shapes of all PUT-*x* did not change at all even after soaking in normal saline for 30 days; as for the appearances, only PUT-0 and PUT-3 underwent a slight change from transparent to white, whereas the appearances of PUT-5 and PUT-10 changed little. The retentions of the shape and appearance of the PUT-5 and PUT-10 specimens could be regarded as intuitional evidence of good resistance toward human sweat. Furthermore, it should be noted that the water resistance of the PUT-5 and PUT-10 is much better than that of the commercialized 1180A, which severely lost its original shape and appearance after soaking in deionized water for 3 days.<sup>7</sup> It is a common sense that the saline permeates the PU film along its thickness, and the more winding diffusion pathway for saline, the more penetration time it takes.<sup>73</sup> In terms of PUT-5 and PUT-10, they contain more benzene rings compared with the

PUT-0 and PUT-3, thus more compact microstructures caused by more  $\pi$ - $\pi$  interactions can be anticipated in PUT-5 and PUT-10 than those in PUT-0 and PUT-3, which effectively delays the permeation of the saline.<sup>74</sup>

To further explore the potential application of self-healing polyurethane materials obtained in this work, a fluorescent anti-counterfeiting film was fabricated by using the PUT-5 as the matrix (Figure 10(d)). The anti-counterfeiting film showed a yellow appearance under the ambient condition (Figure 10(d-i)), and displayed red emission under 365 nm excitation (Figure 10(d-ii)). To testify the durability of the anti-counterfeiting and self-healing of the film, it was cut into two pieces after storage at an aging oven for 30 days, and the obvious change is the appearance which changed from yellow to light yellow under the natural light (Figure 10(d-iii)). Interestingly, red fluorescence emission again overtly appeared under the UV excitation (Figure 10(d-iv)). Moreover, the damage caused by cutting was fully self-healed after self-healing at 80 °C for 1h (Figure 10(d-v)), and its anti-counterfeiting ability was also well maintained (Figure 10(d-vi)). Taking advantage of unique self-healing property and durability, the PUT-5 is a qualified matrix for preparing anti-counterfeiting materials. Moreover, the above research provides a new idea for the development of new self-healing anti-counterfeiting materials, expanding the application of the polyurethane in the anti-counterfeiting field.

## Conclusions

In summary, by controlling the ratio of TDI and IPDI, we designed and synthesized a series of self-healing PUT-*x* systems, and especially the PUT-5 possess outstanding and distinct features of favorable self-healing ability, admirable mechanical property and agreeable appearance, and based on the performances of the PUT-5, we suggest that it has broad application prospects in the fields of self-healing protective coating, anti-counterfeiting material, matrix for wearable electronics, *etc.* Moreover, we also hope that through this work, we can light up on the regulation of the self-healing properties and mechanical properties of the polyurethanes by adjusting the supermolecular forces in the polyurethane molecular chain.

**Acknowledgements:** The authors are grateful for the financial support from by National Natural Science Foundation of China (Grant NO. 21963006), Science and Technology Top Talent Project of Guizhou Provincial Department of Education (Grant NO. Qianjiaohe KY Zi [2020] 036), Natural Science

Foundation of Guizhou Provincial Department of Education (Grant NO. Qianjiaohu KY Zi [2017] 009), High-Level Innovative Talents Project of Guizhou Province (Grant NO. 2018-LIU YUAN and Qiankehe [2019] 5636), Start-Up Foundation of Doctoral Research of Guiyang University (Grant NO. GYU-KY-[2021]), The University of Guizhou Province Engineering Research Center Project (No. KY [2012] 023), Major Science and Technology Project in Guizhou Province (Grant No. Q.K.H.Z.D.Z.X.Z [2019] 3016), Innovation and Entrepreneurship Training for College Students of Guiyang University (Grant NO. 2020-LIU YUAN), Science and Technology Planning Project of Guiyang City [NO. [2020]37-3]; Natural Science Foundation of Guizhou (Grant NO. Qiankehe-ZK[2022] KEY002). The raw/processed data required to reproduce these findings cannot be shared at this time due to technical or time limitations.

**Conflicts of Interest:** There are no conflicts of interest to declare.

**Supporting Information:** <sup>1</sup>H-NMR spectra of PUT-*x* (Figure S1), FTIR spectra of PUT-*x* (Figure S2), DTG curves of the prepared PUT-*x* (Figure S3), Digital images of the PUT-*x* (Figure S4), UV-Vis reflection spectra of the PUT-*x* (Figure S5), Optical microscopic images of healing process for a scratch in PUT-*x* (Figure S6-S8), Digital images of the tensile tests of scratched PUT-*x* after being healed at 80 °C for 30 min (Figure S9-S11), Strain vs. stress curves of scissored PUT-*x* specimens (Figure S12-S13), Temperature-dependent transmission FTIR spectra of PUT-0, PUT-5 and PUT-10 (Figure S14), Digital image of the PUT-10 turns into a gel (Figure S15), UV-Vis spectra of the PUT-*x* in tetrahydrofuran (Figure S16), Feeding amount of the raw materials of PUT-*x* (Table S1), Mass contents of the hard segments and TDI in PUT-*x* (Table S2), Percentage of the H-bonded C=O in PUT-0, PUT-5 and PUT-10 (Table S3). The materials are available *via* the Internet at <http://journal.polymer-korea.or.kr>.

## References

1. Wu, P. X.; Cheng, H. Y.; Wang, X. C.; Shi, R. H.; Zhang, C.; Arai, M.; Zhao, F. Y. A Self-healing and Recyclable Polyurethane-urea Diels-Alder Adduct Synthesized from Carbon Dioxide and Furfuryl Amine. *Green Chem.* **2021**, *23*, 552-560.
2. Zhang, K.; Sun, J.; Song, J.; Gao, C.; Wang, Z.; Song, C.; Wu, Y.; Liu, Y. Self-Healing Ti<sub>3</sub>C<sub>2</sub> MXene/PDMS Supramolecular Elastomers Based on Small Biomolecules Modification for Wearable Sensors. *ACS Appl. Mater. Interfaces* **2020**, *12*, 45306-45314.
3. Döhler, D.; Kang, J.; Cooper, C. B.; Tok, J. B. H.; Rupp, H.; Binder, W. H.; Bao, Z. Tuning the Self-Healing Response of Poly(dimethylsiloxane)-Based Elastomers. *ACS Appl. Polym. Mater.* **2020**, *2*, 4127-4139.
4. Fan, J.; Huang, J.; Gong, Z.; Cao, L.; Chen, Y. Toward Robust, Tough, Self-Healable Supramolecular Elastomers for Potential Application in Flexible Substrates. *ACS Appl. Mater. Interfaces* **2020**, *12*, 1135-1144.
5. Samadzadeh, M.; Boura, S. H.; Peikari, M.; Ashrafi, A.; Kasiriha, M. Tung Oil: An Autonomous Repairing Agent for Self-healing Epoxy Coatings. *Prog. Org. Coat.* **2011**, *70*, 383-387.
6. Hu, Z.; Zhang, D.; Lu, F.; Yuan, W.; Xu, X.; Zhang, Q.; Liu, H.; Shao, Q.; Guo, Z.; Huang, Y. Multistimuli-Responsive Intrinsic Self-Healing Epoxy Resin Constructed by Host-Guest Interactions. *Macromolecules* **2018**, *51*, 5294-5303.
7. Ying, W. B.; Yu, Z.; Kim, D. H.; Lee, K. J.; Hu, H.; Liu, Y.; Kong, Z.; Wang, K.; Shang, J.; Zhang, R.; Zhu, J.; Li, R. W. Waterproof, Highly Tough, and Fast Self-Healing Polyurethane for Durable Electronic Skin. *ACS Appl. Mater. Interfaces* **2020**, *12*, 11072-11083.
8. Chang, K.; Jia, H.; Gu, S.-Y. A Transparent, Highly Stretchable, Self-healing Polyurethane Based on Disulfide Bonds. *Eur. Polym. J.* **2019**, *112*, 822-831.
9. Zhang, X. T.; Wang, S. J.; Jiang, Z. K.; Li, Y.; Jing, X. L. Boronic Ester Based Vitrimers with Enhanced Stability via Internal Boron-Nitrogen Coordination. *J. Am. Chem. Soc.* **2020**, *142*, 21852-21860.
10. Li, Y.; Yang, L.; Zeng, Y.; Wu, Y.; Wei, Y.; Tao, L. Self-Healing Hydrogel with a Double Dynamic Network Comprising Imine and Borate Ester Linkages. *Chem. Mater.* **2019**, *31*, 5576-5583.
11. Chao, A.; Negulescu, I.; Zhang, D. Dynamic Covalent Polymer Networks Based on Degenerative Imine Bond Exchange: Tuning the Malleability and Self-Healing Properties by Solvent. *Macromolecules* **2016**, *49*, 6277-6284.
12. Kathan, M.; Kovaříček, P.; Jurissek, C.; Senf, A.; Dallmann, A.; Thünemann, A. F.; Hecht, S. Control of Imine Exchange Kinetics with Photoswitches to Modulate Self-Healing in Polysiloxane Networks by Light Illumination. *Angew. Chem. Int. Ed.* **2016**, *55*, 13882-13886.
13. Li, X.; Yu, R.; He, Y.; Zhang, Y.; Yang, X.; Zhao, X.; Huang, W. Self-Healing Polyurethane Elastomers Based on a Disulfide Bond by Digital Light Processing 3D Printing. *ACS Macro Lett.* **2019**, *8*, 1511-1516.
14. Fang, Y.; Du, X.; Jiang, Y.; Du, Z.; Pan, P.; Cheng, X.; Wang, H. Thermal-Driven Self-Healing and Recyclable Waterborne Polyurethane Films Based on Reversible Covalent Interaction. *ACS Sustainable Chem. Eng.* **2018**, *6*, 14490-14500.
15. Wang, J. K.; Lv, C.; Li, Z. X.; Zheng, J. P. Facile Preparation of Polydimethylsiloxane Elastomer with Self-Healing Property and Remoldability Based on Diels-Alder Chemistry. *Macromol. Mater. Eng.* **2018**, *303*, 1800089.
16. Li, Y.; Li, W.; Sun, A.; Jing, M.; Liu, X.; Wei, L.; Wu, K.; Fu, Q. A Self-reinforcing and Self-healing Elastomer with High Strength, Unprecedented Toughness and Room-temperature Reparability. *Mater. Horiz.* **2020**, *8*, 267-275.

17. Tamate, R.; Hashimoto, K.; Horii, T.; Hirasawa, M.; Li, X.; Shibayama, M.; Watanabe, M. Self-Healing Micellar Ion Gels Based on Multiple Hydrogen Bonding. *Adv. Mater.* **2018**, *30*, 1802792.
18. Li, L.; Yan, B.; Yang, J.; Chen, L.; Zeng, H. Novel Mussel-Inspired Injectable Self-Healing Hydrogel with Anti-Biofouling Property. *Adv. Mater.* **2015**, *27*, 1294-1299.
19. Li, X.; Huang, X.; Mutlu, H.; Malik, S.; Theato, P. Conductive Hydrogel Composites with Autonomous Self-healing Properties. *Soft Matter* **2020**, *16*, 10969-10976.
20. Sun, Y.; Ren, Y.-Y.; Li, Q.; Shi, R.-W.; Hu, Y.; Guo, J.-N.; Sun, Z.; Yan, F. Conductive, Stretchable, and Self-healing Ionic Gel Based on Dynamic Covalent Bonds and Electrostatic Interaction. *Chin. J. Polym. Sci.* **2019**, *37*, 1053-1059.
21. Liu, Y.; Li, Z.; Liu, R.; Liang, Z.; Yang, J.; Zhang, R.; Zhou, Z.; Nie, Y. Design of Self-Healing Rubber by Introducing Ionic Interaction To Construct a Network Composed of Ionic and Covalent Cross-Linking. *Ind. Eng. Chem. Res.* **2019**, *58*, 14848-14858.
22. Liu, X.; Liu, X.; Li, W.; Ru, Y.; Li, Y.; Sun, A.; Wei, L. Engineered Self-healable Elastomer with Giant Strength and Toughness via Phase Regulation and Mechano-responsive Self-reinforcing. *Chem. Eng. J.* **2021**, *410*, 128300.
23. Li, Y.; Yang, Z.; Zhang, J.; Ding, L.; Pan, L.; Huang, C.; Zheng, X.; Zeng, C.; Lin, C. Novel Polyurethane with High Self-healing Efficiency for Functional Energetic Composites. *Polym. Test.* **2019**, *76*, 82-89.
24. Wan, T.; Chen, D. Mechanical Enhancement of Self-healing Waterborne Polyurethane by Graphene Oxide. *Prog. Org. Coat.* **2018**, *121*, 73-79.
25. Chen, X.; Zhu, J.; Luo, Y.; Chen, J.; Ma, X.; Bukhvalov, D.; Liu, H.; Zhang, M.; Luo, Z. Molecular Dynamics Simulation Insight into the Temperature Dependence and Healing Mechanism of an Intrinsic Self-healing Polyurethane Elastomer. *Phys. Chem. Chem. Phys.* **2020**, *22*, 17620-17631.
26. Liang, Z.; Huang, D.; Zhao, L.; Nie, Y.; Zhou, Z.; Hao, T.; Li, S. Self-healing Polyurethane Elastomer Based on Molecular Design: Combination of Reversible Hydrogen Bonds and High Segment Mobility. *J. Inorg. Organomet. Polym. Mater.* **2020**, *31*, 683-694.
27. Petrović, Z. S.; Ferguson, J. Polyurethane elastomers. *Prog. Polym. Sci.* **1991**, *16*, 695-836.
28. Liang, Z.; Huang, D.; Zhao, L.; Nie, Y.; Zhou, Z.; Hao, T.; Li, S. Self-healing Polyurethane Elastomer Based on Molecular Design: Combination of Reversible Hydrogen Bonds and High Segment Mobility. *J. Inorg. Organomet. Polym. Mater.* **2020**, *31*, 683-694.
29. ACS Appl Mater Interfaces Zhang, L.; Liu, Z.; Wu, X.; Guan, Q.; Chen, S.; Sun, L.; Guo, Y.; Wang, S.; Song, J.; Jeffries, E. M.; He, C.; Qing, F. L.; Bao, X.; You, Z. A Highly Efficient Self-Healing Elastomer with Unprecedented Mechanical Properties. *Adv. Mater.* **2019**, *31*, e1901402.
30. Patel, J.; Bahadur, A. Histopathological Manifestations of sub Lethal Toxicity of Copper Ions in Catla Catla. *AEJTS* **2011**, *3*, 1-5.
31. Stauber, J.; Florence, T. Mechanism of Toxicity of Ionic Copper and Copper Complexes to Algae. *Mar. Biol.* **1987**, *94*, 511-519.
32. Joram Mendoza, D.; Mouterde, L. M. M.; Browne, C.; Singh Raghuwanshi, V.; Simon, G. P.; Garnier, G.; Allais, F. Grafting Nature-Inspired and Bio-Based Phenolic Esters onto Cellulose Nanocrystals Gives Biomaterials with Photostable Anti-UV Properties. *ChemSusChem* **2020**, *13*, 6552-6561.
33. Zhang, T.; Deng, Y.; Zhang, W.; Wang, G.; Zhong, Y.; Su, C.; Li, H. A Self-colored Waterborne Polyurethane Film with Natural Curcumin as a Chain Extender and Excellent UV-Absorbing Properties. *Polymer* **2022**, *239*, 124465.
34. Zhou, J.; Liu, H.; Sun, Y.; Wang, C.; Chen, K. Self-Healing Titanium Dioxide Nanocapsules-Graphene/Multi-Branched Polyurethane Hybrid Flexible Film with Multifunctional Properties toward Wearable Electronics. *Adv. Funct. Mater.* **2021**, *31*, 2011133.
35. More, A. S.; Gadenne, B.; Alfos, C.; Cramail, H. AB Type Polyaddition Route to Thermoplastic Polyurethanes from Fatty Acid Derivatives. *Polym. Chem.* **2012**, *3*, 1594-1605.
36. Yang, S.; Wang, S.; Du, X.; Cheng, X.; Wang, H.; Du, Z. Mechanically and Thermo-driven Self-healing Polyurethane Elastomeric Composites Using Inorganic-organic Hybrid Material as Crosslinker. *Polym. Chem.* **2020**, *11*, 1161-1170.
37. Song, P.; Xu, Z.; Wu, Y.; Cheng, Q.; Guo, Q.; Wang, H. Super-tough Artificial Nacre Based on Graphene Oxide via Synergistic Interface Interactions of  $\pi$ - $\pi$  Stacking and Hydrogen Bonding. *Carbon* **2017**, *111*, 807-812.
38. Lai, Y.; Kuang, X.; Yang, W.-H.; Wang, Y.; Zhu, P.; Li, J.-P.; Dong, X.; Wang, D.-J. Dynamic Bonds Mediate  $\pi$ - $\pi$  Interaction via Phase Locking Effect for Enhanced Heat Resistant Thermoplastic Polyurethane. *Chin. J. Polym. Sci.* **2020**, *39*, 154-163.
39. Biswas, A.; Kim, S.; He, Z.; Cheng, H. N. Microwave-Assisted Synthesis and Characterization of Polyurethanes from TDI and Starch. *Int. J. Polym. Anal. Charact.* **2015**, *20*, 1-9.
40. Wang, S.; Yang, Y.; Ying, H.; Jing, X.; Wang, B.; Zhang, Y.; Cheng, J. Recyclable, Self-Healable, and Highly Malleable Poly(urethane-urea)s with Improved Thermal and Mechanical Performances. *ACS Appl. Mater. Interfaces* **2020**, *12*, 35403-35414.
41. Yao, W.; Tian, Q.; Shi, J.; Luo, C.; Wu, W. Printable, Down/Up-Conversion Triple-Mode Fluorescence Responsive and Colorless Self-Healing Elastomers with Superior Toughness. *Adv. Funct. Mater.* **2021**, *31*, 2100211.
42. Tang, Q.; Gao, K. Structure Analysis of Polyether-based Thermoplastic Polyurethane Elastomers by FTIR,  $^1\text{H}$  NMR and  $^{13}\text{C}$  NMR. *Int. J. Polym. Anal. Charact.* **2017**, *22*, 569-574.
43. Sugane, K.; Shibata, M. Self-healing Thermoset Polyurethanes Utilizing Host-guest Interaction of Cyclodextrin and Adamantane. *Polymer* **2021**, *221*, 123629.
44. Liu, Y.; Zhao, J.; Peng, Y.; Luo, J.; Cao, L.; Liu, X. Comparative Study on the Properties of Epoxy Derived from Aromatic and Heteroaromatic Compounds: The Role of Hydrogen Bonding. *Ind. Eng. Chem. Res.* **2020**, *59*, 1914-1924.
45. Liu, Y.; Li, C.; Dai, J.; Jiang, Y.; Liu, X.; Zhu, J. Synthesis of Multifunctional Monomers from Rosin for the Properties Enhancement of Soybean-oil Based Thermosets. *Sci. China: Technol. Sci.* **2017**, *60*, 1332-1338.
46. Favero, D.; Marcon, V.; Figueroa, C. A.; Gómez, C. M.; Cros, A.; Garro, N.; Sanchis, M. J.; Carsí, M.; Bianchi, O. Effect of Chain Extender on the Morphology, Thermal, Viscoelastic, and Dielectric

- Behavior of Soybean Polyurethane. *J. Appl. Polym. Sci.* **2021**, 138, 50709.
47. Hao, Y.; Pan, Y.; Du, R.; Wang, Y.; Chen, Z.; Zhang, X.; Wang, X. The Influence of a Thermal Treatment on the Decay Resistance of Wood via FTIR Analysis. *Adv. Mater. Sci. Eng.* **2018**, 2018, 1-7.
  48. Liang, H.; Xie, F.; Liu, M.; Jin, Z.; Luo, F.; Zhang, Z. Luminescence Studies of Europium Chelates with Increasing Benzene Ring Substituents Ligand-doped Polymer. *Spectrochimica Acta Part A: Molecular and Biomolecular Spectroscopy* **2008**, 71, 588-591.
  49. Lu, Y.; Liu, L.; Tian, M.; Geng, H.; Zhang, L. Study on Mechanical Properties of Elastomers Reinforced by Zinc Dimethacrylate. *Eur. Polym. J.* **2005**, 41, 589-598.
  50. Fan, J.; Huang, J.; Gong, Z.; Cao, L.; Chen, Y. Toward Robust, Tough, Self-Healable Supramolecular Elastomers for Potential Application in Flexible Substrates. *ACS Appl. Mater. Interfaces* **2020**, 13, 1135-1144.
  51. Xu, Y.; Chen, D. A Novel Self-Healing Polyurethane Based on Disulfide Bonds. *Macromol. Chem. Phys.* **2016**, 217, 1191-1196.
  52. Ling, J.; Rong, M. Z.; Zhang, M. Q. Photo-stimulated Self-healing Polyurethane Containing Dihydroxyl Coumarin Derivatives. *Polymer* **2012**, 53, 2691-2698.
  53. Yuan, C. E.; Rong, M. Z.; Zhang, M. Q. Self-healing Polyurethane Elastomer with Thermally Reversible Alkoxyamines as Crosslinkages. *Polymer* **2014**, 55, 1782-1791.
  54. Fu, D.; Pu, W.; Wang, Z.; Lu, X.; Sun, S.; Yu, C.; Xia, H. A Facile Dynamic Crosslinked Healable Poly(oxime-urethane) Elastomer with High Elastic Recovery and Recyclability. *J. Mater. Chem. A* **2018**, 6, 18154-18164.
  55. Aranguren, M. I.; González, J. F.; Mosiewicki, M. A. Biodegradation of a Vegetable Oil Based Polyurethane and Wood Flour Composites. *Polym. Test.* **2012**, 31, 7-15.
  56. Gaina, C.; Gaina, V.; Ciobanu, C. Thermal and Mechanical Characterization of Maleimide-functionalized Copoly(urethane-urea)s. *J. Appl. Polym. Sci.* **2009**, 113, 3245-3254.
  57. Rong, J.; Zhong, J.; Yan, W.; Liu, M.; Zhang, Y.; Qiao, Y.; Fu, C.; Gao, F.; Shen, L.; He, H. Study on Waterborne Self-healing Polyurethane with Dual Dynamic Units of Quadruple Hydrogen Bonding and Disulfide Bonds. *Polymer* **2021**, 221, 123625.
  58. Hentschel, T.; Münstedt, H. Kinetics of the Molar Mass Decrease in a Polyurethane Melt: A Rheological Study. *Polymer* **2001**, 42, 3195-3203.
  59. Wang, Y.; Yi, J.; Peng, X.; Ma, X.; Peng, S. Structure-property Relationships of Novel Fluorinated Polycarbonate Polyurethane Films with High Transparency and Thermal Stability. *Res. Chem. Intermed.* **2019**, 45, 845-862.
  60. Chen, P. H.; Yang, Y. F.; Lee, D.-K.; Lin, Y.-F.; Wang, H.-H.; Tsai, H.-B.; Tsai, R.-S. Synthesis and Properties of Transparent Thermoplastic Segmented Polyurethanes. *Adv. Polym. Technol.* **2007**, 26, 33-40.
  61. Hu, J.; Yang, R.; Zhang, L.; Chen, Y.; Sheng, X.; Zhang, X. Robust, Transparent, and Self-healable Polyurethane Elastomer via Dynamic Crosslinking of Phenol-carbamate Bonds. *Polymer* **2021**, 222, 123674.
  62. Burattini, S.; Greenland, B. W.; Merino, D. H.; Weng, W.; Seppala, J.; Colquhoun, H. M.; Hayes, W.; Mackay, M. E.; Hamley, I. W.; Rowan, S. J. A Healable Supramolecular Polymer Blend Based on Aromatic  $\pi$ - $\pi$  Stacking and Hydrogen-Bonding Interactions. *J. Am. Chem. Soc.* **2010**, 132, 12051-12058.
  63. Liu, Y.; Peng, Y.; Luo, J.; Liu, J.; Liu, X. Investigation on the Effects of Bridging Groups in Aromatic Diphenol-Based Benzoxazines: Curing Reaction and H Bonds. *Ind. Eng. Chem. Res.* **2020**, 59, 12085-12095.
  64. Guo, Y.; Zhang, R.; Xiao, Q.; Guo, H.; Wang, Z.; Li, X.; Chen, J.; Zhu, J. Asynchronous Fracture of Hierarchical Microstructures in Hard Domain of Thermoplastic Polyurethane Elastomer: Effect of Chain Extender. *Polymer* **2018**, 138, 242-254.
  65. Feula, A.; Pethybridge, A.; Giannakopoulos, I.; Tang, X.; Chippindale, A.; Siviour, C. R.; Buckley, C. P.; Hamley, I. W.; Hayes, W. A Thermoreversible Supramolecular Polyurethane with Excellent Healing Ability at 45 °C. *Macromolecules* **2015**, 48, 6132-6141.
  66. Gu, Y.-F.; Liu, X.-T.; Zhang, Y.; Zhang, S.-M.; Chang, Z.; Bu, X.-H. Supramolecular Recognition of Benzene Homologues in a 2D Coordination Polymer Through Variable Inter-layer  $\pi$ - $\pi$  Interaction. *CrystEngComm* **2018**, 20, 3313-3317.
  67. Liang, S.; Li, Y.; Chen, Y.; Yang, J.; Zhu, T.; Zhu, D.; He, C.; Liu, Y.; Handschuh-Wang, S.; Zhou, X. Liquid Metal Sponges for Mechanically Durable, All-soft, Electrical Conductors. *J. Mater. Chem. C* **2017**, 5, 1586-1590.
  68. Ning, N.; Huang, W.; Liu, S.; Zhao, Q.; Zou, H.; Yu, B.; Tian, M.; Zhang, L. Highly Stretchable Liquid Metal/polyurethane Sponge Conductors with Excellent Electrical Conductivity Stability and Good Mechanical Properties. *Composites, Part B* **2019**, 179, 107492.
  69. Chen, G.; Deng, X.; Zhu, L.; Handschuh-Wang, S.; Gan, T.; Wang, B.; Wu, Q.; Fang, H.; Ren, N.; Zhou, X. Recyclable, Weldable, Mechanically Durable, and Programmable Liquid Metal-elastomer Composites. *J. Mater. Chem. A* **2021**, 9, 10953-10965.
  70. Teng, L.; Ye, S.; Handschuh-Wang, S.; Zhou, X.; Gan, T.; Zhou, X. Liquid Metal-Based Transient Circuits for Flexible and Recyclable Electronics. *Adv. Funct. Mater.* **2019**, 29, 1808739.
  71. Huang, Z.; Zeng, Q.; Hui, Y.; Alahi, M. E. E.; Qin, S.; Wu, T. Fast Polymerization of Polydopamine Based on Titanium Dioxide for High-Performance Flexible Electrodes. *ACS Appl. Mater. Interfaces* **2020**, 12, 14495-14506.
  72. Wang, C.; Zheng, Y.; Qiao, K.; Xie, Y.; Zhou, X. An Environmentally Friendly Preparation and Characterization of Waterborne Polyurethane Hydrogels by Polyvinyl Alcohol Physical Cross-linking to Improve Water Absorption. *RSC Adv.* **2015**, 5, 73882-73891.
  73. Qiu, S.; Li, W.; Zheng, W.; Zhao, H.; Wang, L. Synergistic Effect of Polypyrrole-Intercalated Graphene for Enhanced Corrosion Protection of Aqueous Coating in 3.5% NaCl Solution. *ACS Appl. Mater. Interfaces* **2017**, 9, 34294-34304.
  74. Ma, M.; Dai, N.; Liu, X.; Li, C.; Yuan, Q.; Huang, F. Reinforcing the Poly(silylene arylacetylene)s via Strong  $\pi$ - $\pi$  Stacking Interactions. *Polymer* **2021**, 229, 123976.

**Publisher's Note** The Polymer Society of Korea remains neutral with regard to jurisdictional claims in published articles and institutional affiliations.